Philosophical Magazine,
Vol. 85, No. 24, 21 August 2005, 2809–2830

Taylor & Francis
Taylor & Francis Group

Dislocation motion in anisotropic multilayer materials

N. M. GHONIEM* and X. HAN

Department of Mechanical and Aerospace Engineering, University of California, Los Angeles, Los Angeles, CA 90095, USA

(*Received 28 November 2004; in final form 21 March 2005*)

Line integral forms for the elastic field of dislocations in anisotropic, multilayer materials are developed and utilized in Parametric Dislocation Dynamics (PDD) computer simulations. Developed equations account for interface image forces on dislocations as a result of elastic modulus mismatch between adjacent layers. The method is applied to study dislocation motion in multilayer thin films. The operation of dislocation sources, dislocation pileups, confined layer slip (CLS), and the loss of layer confinement are demonstrated for a duplex Cu/Ni system. The strength of a thin film of alternating nanolayers is shown to increase with decreasing layer thickness, and that the maximum strength is determined by the *Koehler barrier* in the absence of coherency strains. For alternating Cu/Ni nanolayers, the dependence of the strength on the duplex layer thickness is found to be consistent with experimental results, down to a layer thickness of $\approx$10 nm.

1. Introduction

Dislocation dynamics (DD) methods have been developed to describe plasticity on the basis of direct numerical simulations of the collective motion of dislocation ensembles, with successful applications to deformation problems at the nano- and micro-scales (e.g. [1–4]). However, the majority of these approaches treat bulk isotropic materials, with a few investigations that account for free surfaces or interfaces (e.g. [5–12]). However, these approaches have limitations, either because they are restricted to the simple case of a planar free surface, treat only isotropic materials, or that they lack sufficient numerical resolution near interfaces and surfaces.

Extension of the DD method to anisotropic bulk crystals demonstrated the importance of elastic anisotropy in the outcome of key dislocation reactions, such as the Frank–Read source operation, dislocation junctions, dipoles and overall microstructure evolution [13]. In anisotropic, multilayer materials, such as nanolayered thin films, the ratio of interface area to volume is high, and dislocations are expected to interact with many interfaces. It is desirable, therefore, to extend the methods of three-dimensional (3D) DD that have been successfully developed for bulk crystals to anisotropic multilayer materials. However, solutions for

*Corresponding author. Email: ghoniem@ucla.edu

Philosophical Magazine
ISSN 1478–6435 print/ISSN 1478–6443 online
http://www.tandf.co.uk/journals
DOI: 10.1080/14786430500155338

the elastic field of 3D dislocations near free surfaces or interfaces are very few, and are not directly suitable for inclusion in the DD framework (e.g. [5, 7, 14–16]).

The elastic field of dislocation loops of general geometry in anisotropic multilayer materials can be determined through a surface integral over the dislocation loop [15, 17, 18], provided that Green's functions are available for the specific geometry. In our recent work [18], the Fourier transform method was used to evaluate Green's functions and their derivatives, which were then utilized in surface integrals to calculate the elastic field of dislocation loops. However, surface integral forms cannot be readily incorporated into DD formulations, which are all based on line integrals for the elastic field, self-, and interaction forces. Hence we wish to determine the elastic field variables in the form of line integrals. This would effectively allow faster computations in anisotropic multilayer materials, and can be used further to extend the DD method to such material systems. In addition to the special case of a dislocation loop in a homogeneous infinite space, a line integral representation of the elastic field due to a general dislocation loop is available only for an isotropic half-space [7].

Nanolayered structures are candidates for applications requiring thin volumes (e.g. micro-electronics, opto-electronics, laser mirrors, etc.), or may be developed for more demanding structural applications (e.g. aircraft, rocket engines, transportation, advanced energy, etc.). In nanolayer materials, which contain many interfaces, most of the present methods would either result in low accuracy for the elastic field variables, especially near the interfaces, or have limitations on their applicability. Experimental research on the deformation behaviour of multilayer nanocrystal composites shows that very high strength and ductility can indeed be obtained, when plastic deformation is restricted to flow in confined small volumes [19–21]. The flow stress in nanolayered structures can approach to within one-third of the theoretical shear strength of order $\mu/30$, where μ is the shear modulus [22]. This possibility raises a host of technological and fundamental considerations related to the maximum strength that can be attained in materials. In principle, plastic flow can be confined to small volumes by controlling the strength and spacing of *engineered* dislocation obstacles at the nanoscale [21, 23]. The high strength, and the length scale of the nanostructure itself may result in new considerations in crystal plasticity [24].

The purpose of the present investigation is to establish a systematic theoretical and computational approach for three-dimensional dislocation motion in anisotropic, multilayer materials. Subsequently, we apply the approach to investigate the influence of elastic property mismatch between layers on the strength of nanolayered materials. In section 2, we develop the essential equations that govern the elastic field of an infinitesimal dislocation segment in an anisotropic multilayered material by using the 2D Fourier transformation method. The elastic field of a general dislocation loop of arbitrary geometry is then evaluated through a line integral along the dislocation loop. Computational procedures are obtained for an anisotropic half-space, two half-spaces, and for a multilayered material in section 3, and the results are incorporated into line integrals for 3D dislocations of arbitrary shape. Dislocation motion in multilayered thin films is then investigated in section 4, where the line integral formulation is utilized in 3D dislocation dynamics

computer simulations. The influence of elastic property mismatch on dislocation motion and interaction forces is finally discussed in section 5.

2. Line integral field equations

For a 3D dislocation loop of general geometry, the displacement vector can be expressed as [17]

$$u_i(\mathbf{x}) = -\int_S C_{jlmn} b_m \frac{\partial}{\partial x'_l} G_{ji}(\mathbf{x}', \mathbf{x}) n_n(\mathbf{x}') \, \mathrm{d}S(\mathbf{x}'), \tag{1}$$

where C_{jlmn} are the elastic moduli, $G_{ji}(\mathbf{x}', \mathbf{x})$ are the Green's functions at $\mathbf{x}'$ due to a point force applied at $\mathbf{x}$, S is an arbitrary surface capping the loop, n_n is a unit normal to S and b_m is the Burgers vector.

The surface integral in equation (1) is valid for a dislocation loop in either homogeneous or inhomogeneous materials, assuming that the elastic Green's functions for a particular geometry and elastic anisotropy are known. There are two main difficulties in using equation (1). First, evaluation of surface integrals for dislocation loops of complex 3D geometry can be computationally demanding and intensive [18]. Second, elastic Green's functions are not explicitly known for inhomogeneous anisotropic materials.

For a dislocation loop in an infinite homogeneous space, the displacement gradient tensor can be reduced to a line integral along the dislocation as [17]

$$u_{i,j}(\mathbf{x})^{\infty} = \oint_L \beta^{\infty}_{jih}(\mathbf{x} - \mathbf{x}') \, \mathrm{d}l_h(\mathbf{x}'), \tag{2}$$

where

$$\beta^{\infty}_{jih}(\mathbf{x} - \mathbf{x}') = C_{klmn} b_m \epsilon_{jnh} G^{\infty}_{ik,l}(\mathbf{x} - \mathbf{x}'), \tag{3}$$

and L and $\mathrm{d}l_h$ are the dislocation line and line element, respectively. The superscript ∞ represents quantities in an infinite space, $f_{,l} = \partial f / \partial x_l$, and ϵ_{jnh} is the usual permutation tensor.

The stress field produced by the dislocation can then be expressed as

$$\sigma_{ij}(\mathbf{x})^{\infty} = \oint_L S^{\infty}_{ijh}(\mathbf{x} - \mathbf{x}') \, \mathrm{d}l_h(\mathbf{x}'), \tag{4}$$

where

$$S^{\infty}_{ijh}(\mathbf{x} - \mathbf{x}') = C_{ijkl} C_{pqmn} \epsilon_{lnh} b_m G^{\infty}_{kp,q}(\mathbf{x} - \mathbf{x}'). \tag{5}$$

The kernel $S^{\infty}_{ijh}(\mathbf{x} - \mathbf{x}')$ in equation (5) can be considered as the ij-stress component at $\mathbf{x}$ produced by a line element of dislocation lying in the h direction at $\mathbf{x}'$, with Burgers vector $\mathbf{b}$ in an infinite space, while $\beta^{\infty}_{jih}(\mathbf{x} - \mathbf{x}')$ in equation (3) can be considered as the corresponding displacement gradient.

For a finite space, the field produced by the elemental dislocation source in an infinite space is not guaranteed to satisfy prescribed boundary conditions.

We therefore need to add a complementary solution (denoted as $S^{\mathrm{C}}_{ijh}(\mathbf{x},\mathbf{x}')$ or $\beta^{\mathrm{C}}_{jih}(\mathbf{x},\mathbf{x}')$) to the infinite medium solution ($S^{\infty}_{ijh}(\mathbf{x}-\mathbf{x}')$ or $\beta^{\infty}_{jih}(\mathbf{x}-\mathbf{x}')$), such that all boundary conditions can be satisfied. For example, on a free surface at $x_3=0$, we should have: $[S^{\infty}_{ijh}(\mathbf{x}-\mathbf{x}')+S^{\mathrm{C}}_{ijh}(\mathbf{x},\mathbf{x}')]|_{x_3=0}=0$. If a complementary solution (with a superscript C) can be obtained, then the elastic field due to a dislocation loop in the corresponding finite space can be evaluated through the line integral:

$$u_{i,j}(\mathbf{x})=\oint_L[\beta^{\infty}_{jih}(\mathbf{x}-\mathbf{x}')+\beta^{\mathrm{C}}_{jih}(\mathbf{x},\mathbf{x}')]\,\mathrm{d}l_h(\mathbf{x}'), \tag{6}$$

$$\sigma_{ij}(\mathbf{x})=\oint_L[S^{\infty}_{ijh}(\mathbf{x}-\mathbf{x}')+S^{\mathrm{C}}_{ijh}(\mathbf{x},\mathbf{x}')]\,\mathrm{d}l_h(\mathbf{x}'). \tag{7}$$

The first terms in equations (6) and (7) are known infinite space solutions, and contain well-understood singularities. The second (complementary) terms, however, are regular, and need to be determined according to interface and boundary conditions. Now, assume that the displacement field of the complementary kernel is u^{C}_{kh}. The stress field it produces is then: $S^{\mathrm{C}}_{ijh}(\mathbf{x},\mathbf{x}')=C_{ijkl}u^{\mathrm{C}}_{kh,l}(\mathbf{x},\mathbf{x}')$, and the corresponding equilibrium equation is given by

$$C_{ijkl}(\mathbf{x})u^{\mathrm{C}}_{kh,lj}(\mathbf{x},\mathbf{x}')=0. \tag{8}$$

For a layered medium, the general solution can be obtained by a Fourier transform with respect to the in-plane coordinates (x_1,x_2) as [18]

$$\tilde{\mathbf{u}}(\xi_1,\xi_2,x_3;x_3')=\int_0^{\infty}\int_0^{\infty}\mathbf{u}(\mathbf{x};(0,0,x_3'))e^{\mathbf{i}\xi_\alpha x_\alpha}\,\mathrm{d}x_1\,\mathrm{d}x_2. \tag{9}$$

The equilibrium equation then becomes

$$C_{i3k3}\tilde{u}^{\mathrm{C}}_{kh,33}-\mathbf{i}(C_{i\alpha k3}+C_{i3k\alpha})\xi_\alpha\tilde{u}^{\mathrm{C}}_{kh,3}-C_{i\alpha k\beta}\xi_\alpha\xi_\beta\tilde{u}^{\mathrm{C}}_{kh}=0, \tag{10}$$

where the Greek subscript $\alpha=1$ or 2, whereas Roman subscripts range over 1, 2, 3.

The general solution of equation (10) can be expressed in a compact form as [25]

$$\tilde{\mathbf{u}}^{\mathrm{C}}(\xi_1,\xi_2,x_3;x_3')=\mathbf{i}\eta^{-1}(\bar{\mathbf{A}}\langle e^{-\mathbf{i}\bar{\mathbf{p}}\eta x_3}\rangle\mathbf{V}+\mathbf{A}\langle e^{-\mathbf{i}\mathbf{p}\eta x_3}\rangle\mathbf{W}), \tag{11}$$

where (η,θ) are the polar coordinates of (ξ_1,ξ_2) ($\xi_1=\eta\cos\theta$, $\xi_2=\eta\sin\theta$), $\mathbf{V}$ and $\mathbf{W}$ are unknown functions (of η, θ and x_3'), and $\langle e^{-\mathbf{i}\mathbf{p}\eta x_3}\rangle=\mathrm{diag}[e^{-\mathbf{i}p_1\eta x_3},e^{-\mathbf{i}p_2\eta x_3},e^{-\mathbf{i}p_3\eta x_3}]$. p_i ($\mathrm{Im}(p_i)>0$) and $\mathbf{A}=(\mathbf{a}_1,\mathbf{a}_2,\mathbf{a}_3)$ are the eigenvalues and eigenmatrix of the generalized Stroh eigenproblem [26]:

$$[\mathbf{Q}+p_i\mathbf{R}+\mathbf{R}^{\mathrm{T}})+p_i^2\mathbf{T}]\mathbf{a}_i=0, \tag{12}$$

$$Q_{ik}=C_{ijks}n_jn_s,\quad R_{ik}=C_{ijks}n_jm_s,\quad T_{ik}=C_{ijks}m_jm_s,$$

with $\mathbf{n}=[\cos\theta,\sin\theta,0]^{\mathrm{T}}$ and $\mathbf{m}=[0,0,1]^{\mathrm{T}}$.

The displacement gradient for the complementary solution is

$$\tilde{\mathbf{u}}^{\mathrm{C}}_{,\alpha}(\xi_1,\xi_2,x_3;x_3')=n_\alpha(\bar{\mathbf{A}}\langle e^{-\mathbf{i}\bar{\mathbf{p}}\eta x_3}\rangle\mathbf{V}+\mathbf{A}\langle e^{-\mathbf{i}\mathbf{p}\eta x_3}\rangle\mathbf{W}). \tag{13}$$

The induced stress field will then be: $S^{\mathrm{C}}_{ijh}(\mathbf{x},\mathbf{x}') = C_{ijkl}u^{\mathrm{C}}_{kh,\,l}(\mathbf{x},\mathbf{x}')$. We will separate the field into two contributions: (1) out-of-plane stresses $\mathbf{t} = (S_{13h}, S_{23h}, S_{33h})$, and (2) in-plane stresses $\mathbf{s} = (S_{11h}, S_{12h}, S_{22h})$. In the transformed domain, these can be expressed as [25]

$$\tilde{\mathbf{t}}^{\mathrm{C}}(\xi_1,\xi_2,x_3;x_3') = \bar{\mathbf{B}}\langle e^{-\mathbf{i}\bar{\mathbf{p}}\eta x_3}\rangle\mathbf{V} + \mathbf{B}\langle e^{-\mathbf{i}\mathbf{p}\eta x_3}\rangle\mathbf{W}, \tag{14}$$

$$\tilde{\mathbf{s}}^{\mathrm{C}}(\xi_1,\xi_2,x_3;x_3') = \bar{\mathbf{C}}\langle e^{-\mathbf{i}\bar{\mathbf{p}}\eta x_3}\rangle\mathbf{V} + \mathbf{C}\langle e^{-\mathbf{i}\mathbf{p}\eta x_3}\rangle\mathbf{W}. \tag{15}$$

The matrices $\mathbf{B} = (\mathbf{b}_1,\mathbf{b}_2,\mathbf{b}_3)$ and $\mathbf{C} = (\mathbf{c}_1,\mathbf{c}_2,\mathbf{c}_3)$ are related to the Stroh eigenmatrix $\mathbf{A}$ as

$$\mathbf{b}_i = (\mathbf{R}^{\mathrm{T}} + p_i\mathbf{T})\mathbf{a}_i, \quad \mathbf{c}_i = \mathbf{D}_i\mathbf{a}_i, \tag{16}$$

with

$$D_{kli} = C_{1kl\alpha}n_\alpha + p_iC_{1kl3} \quad \text{for } k = 1,2, \quad \text{and } D_{3li} = C_{22l\alpha}n_\alpha + p_iC_{22l3}.$$

Note that for a half-space $x_3 \le 0$, $V = 0$, while for $x_3 \ge 0$, $W = 0$.

In order to impose the appropriate boundary conditions for layered materials, the transformed Green's tensor in an infinite space is needed. This is given by

$$\tilde{G}^{\infty}(\xi_1,\xi_2,x_3;x_3') = \mathbf{i}\eta^{-1}\begin{cases} \mathbf{A}\langle e^{-\mathbf{i}\mathbf{p}\eta(x_3-x_3')}\rangle\mathbf{A}^{\mathrm{T}}, & x_3 < x_3', \\ -\bar{\mathbf{A}}\langle e^{-\mathbf{i}\bar{\mathbf{p}}\eta(x_3-x_3')}\rangle\bar{\mathbf{A}}^{\mathrm{T}}, & x_3 > x_3'. \end{cases} \tag{17}$$

3. Solutions of field equations

We determine here the complementary terms necessary for obtaining full solutions for dislocation loops in half-space, bi-materials, and in general anisotropic layered media.

3.1. *Anisotropic half-space*

Let us assume that a dislocation loop is situated in an anisotropic half-space, occupying $x_3 \le 0$ and having a free surface on $x_3 = 0$. The surface equilibrium boundary condition is expressed as

$$\left[S^{\mathrm{C}}_{i3h}(\mathbf{x},\mathbf{x}') + S^{\infty}_{i3h}(\mathbf{x}-\mathbf{x}')\right]|_{x_3=0} = 0. \tag{18}$$

In the transformed domain, we have

$$\tilde{S}^{\mathrm{C}}_{i3h}(\mathbf{x},\mathbf{x}')|_{x_3=0} = \tilde{t}^{\mathrm{C}}_{ih}|_{x_3=0} = \mathbf{BW}, \tag{19}$$

$$\begin{aligned}\tilde{S}^{\infty}_{i3h}(\mathbf{x}-\mathbf{x}') &= C_{i3kl}C_{pqmn}\epsilon_{lnh}b_m\tilde{G}^{\infty}_{kp,\,q}(\mathbf{x}-\mathbf{x}') \\ &= -\mathbf{i}\xi_\alpha C_{i3kl}C_{p\alpha mn}\epsilon_{lnh}b_m\tilde{G}^{\infty}_{kp} + C_{i3kl}C_{p3mn}\epsilon_{lnh}b_m\tilde{G}^{\infty}_{kp,\,3}.\end{aligned} \tag{20}$$

Substituting (17) (for $x_3' < x_3 \leq 0$) into (20), we obtain

$$\tilde{S}^{\infty}_{i3h}|_{x_3=0} = \lambda_{ikhpq}\Big[n_q(-\bar{\mathbf{A}}\langle e^{\mathbf{i}\bar{\mathbf{p}}\eta x_3'}\rangle\bar{\mathbf{A}}^{\mathrm{T}})_{kp} + m_q(-\bar{\mathbf{A}}\langle e^{\mathbf{i}\bar{\mathbf{p}}\eta x_3'}\rangle\langle\bar{\mathbf{p}}\rangle\bar{\mathbf{A}}^{\mathrm{T}})_{kp}\Big], \tag{21}$$

where $\lambda_{ikhpq} = C_{i3kl}C_{pqmn}\epsilon_{lnh}b_m$.
Substituting (19) and (21) into the free traction surface boundary condition (in the transformed domain): $\tilde{S}^{\mathrm{C}}_{i3h}(\mathbf{x},\mathbf{x}')|_{x_3=0} + \tilde{S}^{\infty}_{i3h}|_{x_3=0} = 0$, we get

$$\mathbf{W} = \mathbf{B}^{-1}\lambda_{ikhpq}\Big[n_q(\bar{\mathbf{A}}\langle e^{\mathbf{i}\bar{\mathbf{p}}\eta x_3'}\rangle\bar{\mathbf{A}}^{\mathrm{T}})_{kp} + m_q(\bar{\mathbf{A}}\langle e^{\mathbf{i}\bar{\mathbf{p}}\eta x_3'}\rangle\langle\bar{\mathbf{p}}\rangle\bar{\mathbf{A}}^{\mathrm{T}})_{kp}\Big]. \tag{22}$$

The unknown coefficient $\mathbf{W}$ in the complementary solution is thus determined. Substituting (22) into equations (11), (14) and (15) determines the complementary parts of the displacement vector and stress tensor:

$$\tilde{\mathbf{u}}^{\mathrm{C}}(\xi_1,\xi_2,x_3;x_3') = \mathbf{i}\eta^{-1}\mathbf{A}\langle e^{-\mathbf{i}\mathbf{p}\eta x_3}\rangle\mathbf{W}, \tag{23}$$

$$\tilde{\mathbf{t}}^{\mathrm{C}}(\xi_1,\xi_2,x_3;x_3') = \mathbf{B}\langle e^{-\mathbf{i}\mathbf{p}\eta x_3}\rangle\mathbf{W}, \quad \tilde{\mathbf{s}}^{\mathrm{C}}(\xi_1,\xi_2,x_3;x_3') = \mathbf{C}\langle e^{-\mathbf{i}\mathbf{p}\eta x_3}\rangle\mathbf{W}. \tag{24}$$

Written explicitly in component form, the complementary solution for the displacement vector is

$$\tilde{u}^{\mathrm{C}}_{ih} = \mathbf{i}\eta^{-1}A_{ik_1}e^{-\mathbf{i}p_{k_1}x_3\eta}B^{-1}_{k_1k_2}\lambda_{k_2k_3hk_4k_5}(n_{k_5} + m_{k_5}\bar{p}_{k_6})\bar{A}_{k_3k_6}e^{\mathbf{i}\bar{p}_{k_6}x_3'\eta}\bar{A}^{\mathrm{T}}_{k_6k_4}. \tag{25}$$

Similar forms for the components of the stress tensors are obtained by replacing the first term $\mathbf{i}\eta^{-1}A_{ik_1}$ in equation (25) by B_{ik_1} and C_{ik_1}, to obtain $\tilde{t}^{\mathrm{C}}_{ih}$ and $\tilde{S}^{\mathrm{C}}_{ih}$, respectively.

These are complex explicit expressions, but can be written in the following forms:

$$\tilde{\mathbf{u}}^{\mathrm{C}} = \mathbf{i}\eta^{-1}\mathbf{J_2}\langle e^{-\mathbf{i}\mathbf{r}_1\eta}\rangle\mathbf{J_1}\langle e^{-\mathbf{i}\mathbf{r}_0\eta}\rangle\mathbf{J_0} \tag{26}$$

for the displacement vector, and

$$\tilde{\mathbf{t}}^{\mathrm{C}} = \mathbf{J_2}\langle e^{-\mathbf{i}\mathbf{r}_1\eta}\rangle\mathbf{J_1}\langle e^{-\mathbf{i}\mathbf{r}_0\eta}\rangle\mathbf{J_0} \tag{27}$$

for the traction tensor. The same expression is also obtained for the in-plane tensor $\tilde{\mathbf{S}}$. In equations (26) and (27), the tensors $\mathbf{J_n}(\theta)$ and $\mathbf{r_n}(\theta)$ are independent of η, but are functions of θ. These solutions are in the transformed domain, and need to be transformed back to the physical domain by the inverse Fourier transform:

$$f(x_1 - x_1', x_2 - x_2', x_3, x_3') = \frac{1}{(2\pi)^2}\int_0^{\infty}\int_0^{2\pi}\eta\tilde{f}(\eta,\theta,x_3,x_3') \times e^{-\mathbf{i}\eta[(x_1-x_1')\cos\theta+(x_2-x_2')\sin\theta)]}\,\mathrm{d}\theta\,\mathrm{d}\eta. \tag{28}$$

Carrying out the first integral over $(0 < \eta < \infty)$, the 2D inverse transformation is reduced to a 1D integral [25]. The reduced integrals for the elastic fields are given by

$$u_{ih}^{\mathrm{C}} = \frac{1}{(2\pi)^2} \oint_0^{2\pi} \frac{H_{ih}}{s} \, \mathrm{d}\theta, \tag{29}$$

$$t_{ih}^{\mathrm{C}} = -\frac{1}{(2\pi)^2} \oint_0^{2\pi} \frac{H_{ih}}{s^2} \, \mathrm{d}\theta, \tag{30}$$

with $H_{ih} = (J_{k_2})_2 (J_{k_2 k_1})_1 (J_{k_1})_0$, and $s = (r_{k_2})_1 + (r_{k_1})_0 + (x_1 - x_1') \cos\theta + (x_2 - x_2') \sin\theta$. Note that s_{ih} has the same expression as that of t_{ih}, and that all these functions have their own H_{ih} (different from each other), but share the same s

$$H_{ih} = A_{ik_1} B^{-1}_{k_1 k_2} \lambda_{k_2 k_3 h k_4 k_5} (n_{k_5} + m_{k_5} \bar{p}_{k_6}) \bar{A}_{k_3 k_6} \bar{A}^{\mathrm{T}}_{k_6 k_4}. \tag{31}$$

Replacing the first term A_{ik_1} in equation (31) by B_{ik_1} and C_{ik_1}, we obtain the expression H_{ih} for t_{ih}^{C} and s_{ih}^{C}, respectively. Thus, the complementary parts of the elastic field of a dislocation in a half-space can be evaluated by line integrals over the interval $[0, 2\pi]$. The complementary parts plus the infinite-space solutions are the total elastic fields due to an infinitesimal dislocation segment, and the elastic field due to a dislocation loop is obtained through the line integrals (6) and (7).

We give here an example of a 3D dislocation loop of a simple circular geometry to verify the present line integral method, and to illustrate the main characteristics of dislocation fields near interfaces. Consider a circular dislocation loop in a half-space substrate. The loop lies near a free surface or an interface, as shown in figure 1. To be specific, we take the substrate material, which extends for all $z < 0$, to be an

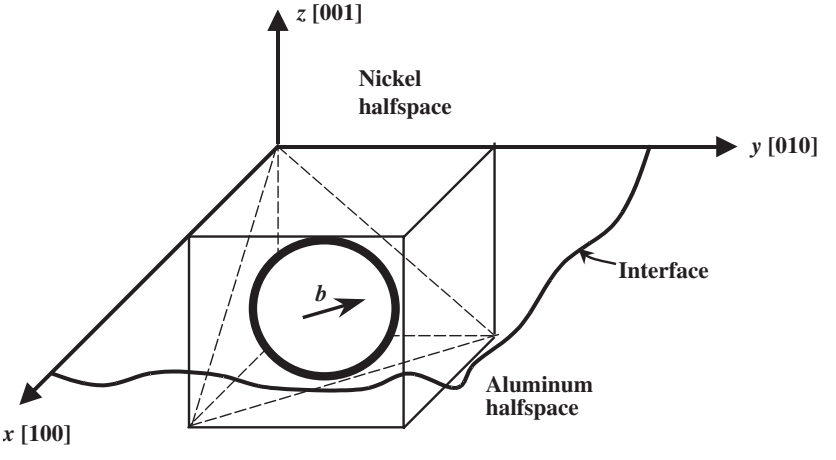

Figure 1. Schematic for the geometry of a 3D circular dislocation loop near an interface or free surface.

anisotropic aluminium crystal. The aluminium substrate is bound by a free surface or is perfectly bonded with an anisotropic nickel half-space along the surface $z=0$. Both Al and Ni are fcc cubic anisotropic crystals (see [27] for elastic constants), with their crystallographic axes [100], [010], and [001] lined up along the $x=1$, $y=2$, and $z=3$ coordinate axes, respectively. The circular dislocation loop lies on the (111) plane, and its Burger's vector $\mathbf{b}$ is taken along the $[\bar{1}10]$ direction. The loop radius $R=200b$, and its centre is located at $z=-180b$, where $b=|\mathbf{b}|$ is the magnitude of the Burgers vector of aluminium.

For verification of the present line integral results, we show in figure 2 the results of stress field components for infinite space and the exact surface integral solutions. Calculations of the surface integral, with equation (1) as the starting point, are performed using an evaluation of Green's functions and their derivatives in the corresponding materials [18]. We follow the procedure of Pan and coworkers for the numerical determination of Green's functions in anisotropic bi-materials and multilayered materials [28, 29]. Stress components along the z axis, induced by the dislocation loop, are shown in figure 2(a) for the case of free surface, and figure 2(b) for the interface case. Because of symmetry, $\sigma_{11}=-\sigma_{22}$, $\sigma_{13}=-\sigma_{23}$, $\sigma_{12}=\sigma_{33}=0$, and thus we only show the stress components σ_{22} and σ_{23}. It can be observed from the figures that the numerical results of the present line integral method are nearly identical to those obtained by the surface integration method [18] for the case of a dislocation in half-space, and are in good agreement when the dislocation loop is near the interface. As the dislocation loop approaches the free surface, the out-of-plane stress components are forced to decrease until they become identically zero at the surface. However, in-plane stresses increase in order to satisfy overall equilibrium. When the aluminium substrate is bonded to a harder half-space (e.g. nickel), out-of-plane stresses are continuous across the interface, and larger than their corresponding values in infinite space. In-plane stress components, on the other hand, experience jumps because of the discontinuity in the elastic properties across the interface. The magnitude of stress increases across the interface, moving from the softer (aluminium) to the harder substrate (nickel).

In general, the stresses near a free surface are larger than their corresponding values near an interface to a harder material. The influence of the interface on the disturbance of the elastic field is somewhat local, and is limited to within a distance of a few hundred lattice constants from the free surface or an interface.

3.2. *Perfectly bonded, anisotropic two half-spaces*

Consider an anisotropic bi-material full space, where the lower half-space ($x_3<0$) is occupied by material (0), the upper half-space ($x_3>0$) by material (1), and quantities in them are denoted by the corresponding superscripts (0) and (1), respectively. Suppose now that the interface (at $x_3=0$) is perfectly bonded. This requires the continuity of the displacement and traction vectors across the interface, i.e.

$$\mathbf{u}^{(0)}|_{x_3=0^-}=\mathbf{u}^{(1)}|_{x_3=0^+},\quad \mathbf{t}^{(0)}|_{x_3=0^-}=\mathbf{t}^{(1)}|_{x_3=0^+}. \tag{32}$$

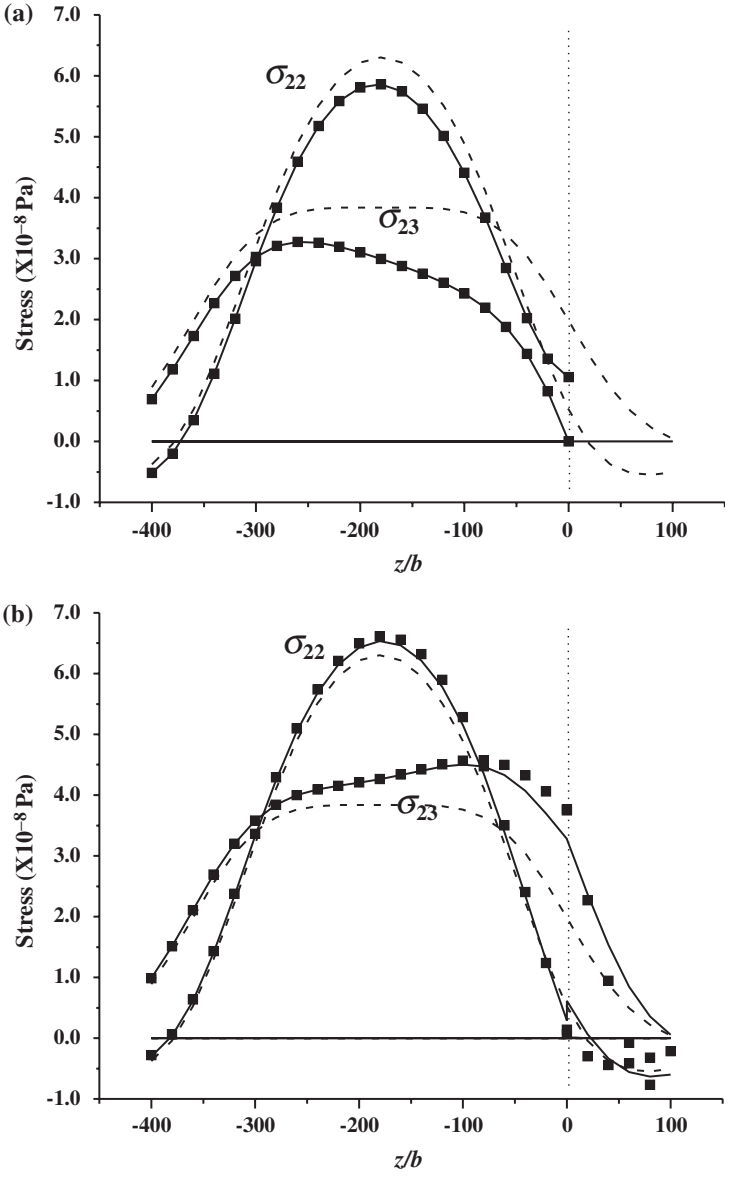

Figure 2. Stress components along the z axis for a circular dislocation loop (see figure 1) in (a) Al half-space and (b) Al–Ni bi-material. Solid lines represent surface integral results, small square symbols, line integral results, and dashed lines, infinite space solutions.

Instead of the displacement continuity condition (32), however, we will use an equivalent condition on the tangential displacement gradient, given by [30]

$$\mathbf{u}^{(0)}_{,\alpha}|_{x_3=0^-} = \mathbf{u}^{(1)}_{,\alpha}|_{x_3=0^+}. \tag{33}$$

Here, $\alpha = 1$ or 2, and $\mathbf{u}_{,\alpha}$ is the in-plane component of the displacement gradient (or so-called tangential distortion).

Without loss of generality, we assume that we have an infinitesimal dislocation segment, located in material (0). We express the solution for the displacement gradient in material (0) as

$$\tilde{\mathbf{u}}^{(0)}_{,j} = \tilde{\mathbf{u}}^{(0)\infty}_{,j} + \tilde{\mathbf{u}}^{(0)\mathrm{C}}_{,j} = \tilde{\boldsymbol{\beta}}^{(0)\infty}_{jih} + n_j \mathbf{A}^{(0)} \langle e^{-\mathrm{i}\mathbf{p}^{(0)}\eta x_3} \rangle \mathbf{W}. \tag{34}$$

The first term $\tilde{\mathbf{u}}^{(0)\infty}_{,j}$ corresponds to the homogeneous full-space solution, which is known from equation (3), with the elastic properties of material (0). The second term corresponds to the complementary solution due to the interface. Correspondingly, the stress field is also separated into two components, and the traction vector can be expressed as

$$\tilde{\mathbf{t}}^{(0)} = \tilde{\mathbf{t}}^{(0)\infty} + \tilde{\mathbf{t}}^{(0)\mathrm{C}} = \tilde{S}^{(0)\infty}_{i3h} + \mathbf{B}^{(0)} \langle e^{-\mathrm{i}\mathbf{p}^{(0)}\eta x_3} \rangle \mathbf{W}, \tag{35}$$

where $S^{(0)\infty}_{i3h}$ is known from equation (5), with the elastic properties of material (0).

Likewise, the solutions in material (1) due to the infinitesimal dislocation segment in material (0) can also be separated. Thus, the displacement gradient in material (1) is expressed as

$$\tilde{\mathbf{u}}^{(1)}_{,j} = \tilde{\mathbf{u}}^{(0)\infty}_{,j} + \tilde{\mathbf{u}}^{(1)\mathrm{C}}_{,j} = \tilde{\boldsymbol{\beta}}^{(0)\infty}_{jih} + n_j \bar{\mathbf{A}}^{(1)} \langle e^{-\mathrm{i}\bar{\mathbf{p}}^{(1)}\eta x_3} \rangle \mathbf{V}. \tag{36}$$

The first term $\tilde{\mathbf{u}}^{(0)\infty}_{,j}$ is the known full-space solution, with the elastic properties of material (0), while the second term is the complementary solution (which is to be determined). The stress field in material (1) can be derived from $\tilde{\mathbf{u}}^{(1)}_{,j}$, giving the traction field as

$$\tilde{\mathbf{t}}^{(1)} = \tilde{\mathbf{t}}^{(1)\infty} + \tilde{\mathbf{t}}^{(1)\mathrm{C}} = \tilde{S}^{(1)\infty}_{i3h} + \bar{\mathbf{B}}^{(1)} \langle e^{-\mathrm{i}\bar{\mathbf{p}}^{(0)}\eta x_3} \rangle \mathbf{V}, \tag{37}$$

with

$$S^{(1)\infty}_{i3h} = C^{(1)}_{ijkl} C^{(0)}_{pqmn} \epsilon_{lnh} b_m G^{(0)\infty}_{kp,q}(\mathbf{x} - \mathbf{x}') \tag{38}$$

as the traction field in full-space material (1) due to the displacement field $\tilde{\mathbf{u}}^{(0)}$.

Substituting equations (34)–(38) into the interface conditions, we have

$$\mathbf{B}^{(0)}\mathbf{W} + \tilde{S}^{(0)\infty}_{i3h}|_{x_3=0} = \bar{\mathbf{B}}^{(1)}\mathbf{V} + \tilde{S}^{(1)\infty}_{i3h}|_{x_3=0}, \tag{39}$$

$$n_\alpha \mathbf{A}^{(0)}\mathbf{W} + \tilde{\boldsymbol{\beta}}^{(0)\infty}_{\alpha ih}|_{x_3=0} = n_\alpha \bar{\mathbf{A}}^{(1)}\mathbf{V} + \tilde{\boldsymbol{\beta}}^{(0)\infty}_{\alpha ih}|_{x_3=0}. \tag{40}$$

Finally, the full solution is obtained as

$$\begin{aligned} \mathbf{W} &= -(\bar{\mathbf{B}}^{(1)}\bar{\mathbf{A}}^{(1)-1}\mathbf{A}^{(0)} - \mathbf{B}^{(0)})^{-1}\Delta\tilde{S}^{\infty}_{i3h}, \\ \mathbf{V} &= (\mathbf{B}^{(0)}\mathbf{A}^{(0)-1}\bar{\mathbf{A}}^{(1)} - \bar{\mathbf{B}}^{(1)})^{-1}\Delta\tilde{S}^{\infty}_{i3h}, \end{aligned} \tag{41}$$

with

$$\Delta\tilde{S}^{\infty}_{i3h} = \tilde{S}^{(1)\infty}_{i3h}|_{x_3=0} - \tilde{S}^{(0)\infty}_{i3h}|_{x_3=0} = (C^{(1)}_{ijkl} - C^{(0)}_{ijkl}) \times C^{(0)}_{pqmn}\epsilon_{lnh}b_m\tilde{G}^{(0)\infty}_{kp,q}(\mathbf{x}-\mathbf{x}')|_{x_3=0},$$

$$\tilde{G}^{(0)\infty}_{kp,q}|_{x_3=0} = -n_q(\bar{\mathbf{A}}^{(0)}\langle e^{\mathbf{i}\bar{\mathbf{p}}^{(0)}\eta x_3'}\rangle\bar{\mathbf{A}}^{(0)\mathrm{T}})_{kp} - m_q \times (\bar{\mathbf{A}}^{(0)}\langle e^{\mathbf{i}\bar{\mathbf{p}}^{(0)}\eta x_3'}\rangle\langle\bar{\mathbf{p}}^{(0)}\rangle\bar{\mathbf{A}}^{(0)T})_{kp}. \quad (42)$$

The displacement and stress (including displacement distortion) solutions have the same forms as equations (26) and (27), respectively, and all real fields are obtained by 1D integrals, as in equations (29) and (30).

Dislocations move along the direction of the Peach–Koehler force exerted on them, which is given by $\mathbf{f} = \boldsymbol{\sigma}\cdot\mathbf{b}\times\mathrm{d}\,\mathbf{l}$, where the virtual force $\mathbf{f}$ is exerted on a line segment $\mathrm{d}\,\mathbf{l}$ with the Burgers vector $\mathbf{b}$, and situated in the stress field $\boldsymbol{\sigma}$. The stress field may originate from various sources, such as applied forces, residual stresses, image stresses (due to boundary conditions), other dislocations, and even the dislocation loop itself (self-forces). When a dislocation resides in a finite medium, adjustments of the stress field to satisfy surface or interface boundary conditions result in local changes of the stress tensor close to the dislocation line. Thus, calculations of the self-force for this altered stress field, which requires integrals along the dislocation line, would also include the influence of the boundary adjustment. Thus, the self-force would subsume the image effects of the boundary, and would be geometry dependent. To remove such ambiguities, and to clearly determine the effects of the interface or boundary, the stress field induced by a dislocation is divided into two parts: the full-space stress $\boldsymbol{\sigma}^{\infty}$, and the image stress $\boldsymbol{\sigma}^{\mathrm{C}}$. The stress $\boldsymbol{\sigma}^{\infty}$ corresponds to that induced by the dislocation in a homogeneous and infinite space, with elastic properties of the material where most of the dislocation resides. The stress field $\boldsymbol{\sigma}^{\infty}$ of a dislocation in an infinite anisotropic material can be calculated by the line integral given by equation (1), and will induce a *self-force* on the dislocation. Because of the singularity of $\boldsymbol{\sigma}^{\infty}$ along the dislocation line, an average field is obtained by the Brown procedure [31], or alternatively through the Gavazza–Barnett limiting process [32]. Details of the numerical procedure for the stress field and self-force of a dislocation loop in an infinite anisotropic material are found in our recent work [13].

The force induced by the complementary part of the stress field, $\boldsymbol{\sigma}^{\mathrm{C}}$, which reflects the interface effect on modifying the infinite medium stress field of the dislocation, will be termed henceforth the *image force*, and is calculated directly by the Peach–Koehler formula. The accuracy of the present line integral method is investigated by a direct comparison with the surface integral method [18] for the Peach–Koehler image force distribution around a general, static and circular dislocation loop near a bi-material interface. In the surface integral method, displacement continuity across the interface is strictly satisfied, while in the present line integral approach, we satisfy an equivalent condition for the continuity of the tangential distortion. However, since the two tangential gradients cannot be simultaneously enforced to be continuous across the interface, one has to select

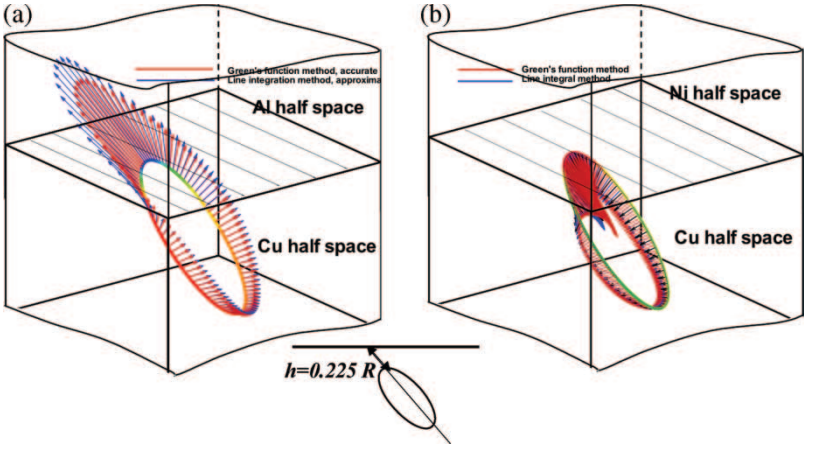

Figure 3. Peach–Koehler force distributions around a circular loop in Cu near a bi-material interface: (a) Cu/Al, and (b) Cu/Ni. Results for the surface integral method (red vectors) are displayed along with those for the current line integral method (blue vectors).

only one of them, and hence obtain an approximate solution. Figure 3 shows the distribution of image forces around a circular loop in Cu, and compares the two methods of calculation. The loop is on a glide plane that is inclined at 45° to the interface. In figure 3(a), image forces are attractive because Al is softer than Cu, while in figure 3(b), forces are repulsive because of the harder Ni half-plane. The agreement between the two methods is satisfactory, both in force direction and magnitude. However, the great simplification of the line integral solution makes it feasible to calculate image forces within the DD framework.

3.3. *Anisotropic multilayer material*

Consider a laterally infinite composite thin film made of different layers. Each layer is homogenous, anisotropic and of uniform thickness. Interfaces between layers are assumed to be perfectly bonded. A coordinate system (x_1, x_2, x_3) is attached to the thin film, with the x_3 axis perpendicular to all interfaces. A general layer n occupies the space $z_{n-1} \le x_3 \le z_n$, and quantities with its properties are denoted by corresponding superscripts (n). Assume now that an infinitesimal dislocation segment is located in layer k. The displacement gradient in layer n can be expressed as

$$\tilde{\mathbf{u}}^{(n)}_{,j} = \tilde{\beta}^{(k)\infty}_{jih} + n_j\Big[\bar{\mathbf{A}}^{(n)}\langle e^{-\mathbf{i}\bar{\mathbf{p}}^{(n)}\eta(x_3-z_{n-1})}\rangle\mathbf{V}^{(n)} + \mathbf{A}^{(n)}\langle e^{-\mathbf{i}\mathbf{p}^{(n)}\eta(x_3-z_n)}\rangle\mathbf{W}^{(n)}\Big]. \tag{43}$$

The first term is the full-space solution, given by equation (3), with the elastic properties of material k. The other terms correspond to the complementary part of the solution. Accordingly, the out-of-plane traction vector is given by

$$\tilde{\mathbf{t}}^{(n)} = \tilde{S}^{(n)\infty}_{i3h} + \Big[\bar{\mathbf{B}}^{(n)}\langle e^{-\mathbf{i}\bar{\mathbf{p}}^{(n)}\eta(x_3-z_{n-1})}\rangle\mathbf{V}^{(n)} + \mathbf{B}^{(n)}\langle e^{-\mathbf{i}\mathbf{p}^{(n)}\eta(x_3-z_n)}\rangle\mathbf{W}^{(n)}\Big], \tag{44}$$

with $S_{i3h}^{(n)\infty} = C_{ijkl}^{(n)} C_{pqmn}^{(k)} \epsilon_{lnh} b_m G_{kp,q}^{(k)\infty}(\mathbf{x} - \mathbf{x}')$, and the solution for the in-plane traction $\tilde{\mathbf{s}}^{(n)}$ is similar to that given by (44).

Perfectly bonded conditions along interfaces require that the traction and displacement (or tangential distortion) vectors are continuous. For interface n, this gives

$$\begin{aligned}\bar{\mathbf{B}}^{(n)} \langle e^{-\mathbf{i}\bar{\mathbf{p}}^{(n)}\eta(z_n - z_{n-1})} \rangle \mathbf{V}^{(n)} + \mathbf{B}^{(n)} \mathbf{W}^{(n)} + \tilde{S}_{i3h}^{(n)\infty}|_{x_3=0} \\ = \bar{\mathbf{B}}^{(n+1)} \mathbf{V}^{(n+1)} + \mathbf{B}^{(n+1)} \langle e^{-\mathbf{i}\mathbf{p}^{(n+1)}\eta(z_n - z_{n+1})} \rangle \mathbf{W}^{(n+1)} + \tilde{S}_{i3h}^{(n+1)\infty}|_{x_3=0},\end{aligned} \tag{45}$$

$$\begin{aligned}\bar{\mathbf{A}}^{(n)} \langle e^{-\mathbf{i}\bar{\mathbf{p}}^{(n)}\eta(z_n - z_{n-1})} \rangle \mathbf{V}^{(n)} + \mathbf{A}^{(n)} \mathbf{W}^{(n)} \\ = \bar{\mathbf{A}}^{(n+1)} \mathbf{V}^{(n+1)} + \mathbf{A}^{(n+1)} \langle e^{-\mathbf{i}\mathbf{p}^{(n+1)}\eta(z_n - z_{n+1})} \rangle \mathbf{W}^{(n+1)}.\end{aligned} \tag{46}$$

With all interface, bottom and top layer (half-space or free surface) boundary conditions, a system of algebraic equations can be formed. Solving these equations, the elastic field is fully determined.

4. Dislocation dynamics in nanolayered materials

In an effort to experimentally explore material parameters that control the strength of nanolayered composites, Cu–Nb, Cu–Cr and Cu–Ni layered structures were produced by cold-working, evaporation or sputtering [20]. In addition, aspects of fcc/bcc duplex structure deformation have recently been considered [33]. The strength increase associated with reduction of the bilayer thickness has been explained by a variety of possible mechanisms, including the Hall–Petch model of dislocation pile-ups at interfaces, the Koehler model of dislocation image interactions, and the Orowan model of single dislocation bow-out between layers. Considering single dislocation behaviour, Embury and Hirth [24] attempted to derive the strength and deformation mechanism maps, allowing for dislocation–dislocation and dislocation–interface interactions. A number of material *design knobs* can be used to impart high strength and control plastic slip in nanolayered structures, including nanolayer height in single crystals, grain size in polycrystals, lattice and interface Peierls stress levels, interface structure, coherency strain level, misfit dislocation structure and spacing, geometry of plastic slip transmission by shear transfer, and the co-deformation of incompatible slip systems (e.g. fcc/bcc, fcc/hcp, and hcp/bcc).

Plastic deformation of nanolayer materials is influenced by the existence of large interfacial areas, as compared to bulk polycrystalline materials. It has been experimentally established that the hardness (or strength) of multilayer thin films is much greater than corresponding bulk materials, and that it increases as the thickness of the constituent layers decreases [20, 34]. Several underlying mechanisms have been proposed in recent years, although relying on approximate treatments of dislocation fields in such systems. The first set of factors that affect strength is structural in nature, where forces on dislocations vary across an interface. The variation can be a result of: (1) lattice constant mismatch that generates coherency strains; (2) misfit interfacial dislocations in semi-coherent and incoherent interfaces;

(3) stacking fault energy changes in incoming and outgoing slip planes; (4) slip system mismatch that forces cross-slip of screw dislocations across the interface; and (5) the effects of dislocation core spreading into the interface [34–36]. The second factor is the mismatch across the interface of elastic properties (constants), which reflect changes in the strength of atomic forces as dislocations cross from one material to another. This *image force* effect places additional opposing forces as dislocations cross an interface, and is known as the *Koehler barrier* (see, for example, [36]). Although the strength of nanolayer materials is dominated by the influence of interfacial image forces on dislocation motion [34–36], current theoretical estimates of image forces on dislocations often rely on approximate methods of analysis based on isotropic, infinitely extended materials. Accurate determination of nanolayer strength and plasticity requires rigorous development of dislocation theory in layered media.

Experimental results and isotropic elasticity estimates show that the dominant mechanism that controls the strength and hardness of multilayer thin films is the influence of the dislocation image force associated with a mismatch in elastic properties between adjacent film layers [34]. For layered materials with a large mismatch in elastic properties, a significant hardness enhancement was observed. On the other hand, for layered materials with small differences in their elastic properties, no measurable hardness enhancement was detected [34]. Experiments on an Fe/Pt layered system [37] indicated that when the bilayer thickness ranges from a few to tens of nanometers, the hardness of this bilayer metal system exhibits a plateau. Over this bilayer period range, the interface structure, misfit dislocation density and coherency strains all change rapidly, so they are not likely to be the dominant mechanism. Hence, the mismatch in elastic moduli was concluded to be the most likely dominant factor determining hardness enhancements in these layered materials [37].

Two models are often used to explain the observed behaviour of hardness (or flow stress) in thin films. In the threading dislocation model [38, 39], the flow stress is determined by the energy balance between the threading glide dislocation segment and the misfit dislocation left behind at the interface. This model results in a flow stress that scales approximately with the inverse of the film/layer thickness. For a thin film/layer of thickness h, subjected to a uniform applied biaxial stress σ_a, the critical stress (σ_c^{th}) for threading dislocation motion (and hence strain relaxation within the layer) is given by [38]

$$\sigma_c^{th} \approx \frac{\mu b}{4\pi(1-\nu)h}[(4-\nu)\ln(h/r_0) - 1] \tag{47}$$

for an isotropic material with a shear modulus μ, Poisson's ration ν, and a dislocation core cut-off radius $r_0 \approx b$. In this model, interfaces are introduced as impenetrable planes for dislocations.

The second model is an extension of the well-known Hall–Petch effect. Here, dislocations are assumed to form a pile-up at a boundary until a critical stress is reached. This results in a flow stress which is inversely proportional to the square root of the layer thickness or grain size. Both models qualitatively explain the

increase in the flow stress with decreasing film/layer thickness, but not the behaviour as the layer thickness decreases below tens of nanometers.

A variational form of the governing equation of motion for a dislocation loop Γ has been developed for over-damped dislocation dynamics, where the work exerted on dislocation loop expansion is balanced by viscous dissipation [4], i.e. $\int_\Gamma (F_k^{\mathrm{t}} - B_{\alpha k} V_\alpha) \delta r_k |\, \mathrm{d}\mathbf{s}| = 0$. Here, F_k^{t} is the total Peach–Koehler force induced by applied external forces, internal stress fields (such as dislocation interactions, interface image forces, and the self-force), $B_{\alpha k}$ is the resistance (inverse mobility) matrix, V_α is the velocity, r_k is the displacement of the dislocation line, and d**s** the dislocation line vector. Because the present formulation results in a line integral form of the force vector distribution, it can be readily incorporated into the PDD framework [4]. In this section, we present computer simulation results for dislocation motion in nanolayered materials using the PDD methodology. We focus on dislocation motion in relatively thin layers, when the individual layer thickness is in the range of a few nanometers to hundreds of nanometers. This is typically much smaller than the characteristic length scale of grains occupied by dislocation networks in bulk materials. Therefore, the number of dislocations needed in order to study thin layer plasticity is small. In many cases, plasticity and strength can be described through the behaviour of a single dislocation loop. Although coherency strains result in a bi-axial in-plane stress state that can be readily included, we do not consider this effect here. We wish to clarify the influence of elastic property mismatch alone on dislocation motion.

Consider a Cu thin layer (thickness h), sandwiched between two semi-infinite, harder Ni substrates. The dislocation is originally located within the thin layer. Cu and Ni are both fcc crystals with [001] out-of-plane orientations and $\langle 110 \rangle \{111\}$ slip systems. In Cu, $b = 0.361$ nm, and the dislocation mobility is taken to be isotropic ($M = 10^4\ \mathrm{Pa}^{-1}\,\mathrm{s}^{-1}$). The system is subjected to a uniform applied biaxial stress σ_{a}. The value of the image force increases as the dislocation segment approaches the interface, and is singular exactly at the interface. This is a consequence of the assumption of linear elasticity, which has been successfully used in dislocation dynamics simulations including similar singular behaviour of the dislocation self-force, energy and junction formation. If a cut-off radius is introduced for the dislocation, the results of infinitesimal linear elasticity for self-force, energy, and junction formation are in good agreement with more detailed atomistic simulations [40]. We assume also here that dislocations do not dissociate into partials, and take the cut-off radius to be $r_0 \approx b$ [38, 39]. Detailed atomistic simulations are required to ascertain the most appropriate value of the cut-off distance [36]. In the following simulations, we assume that there is one Frank–Read (F–R) source inside one of the layers, and that the source dislocation is initially straight and pinned from both ends.

4.1. *Confined layer slip (CLS)*

Figure 4 shows the propagation mode of a source dislocation in a Cu layer of thickness 144 nm at different loading levels. We choose the length L of the original dislocation to be longer than the layer thickness, h, i.e. $L = 4h$. Under a small applied stress below a critical value (approximately estimated by Freund's formula,

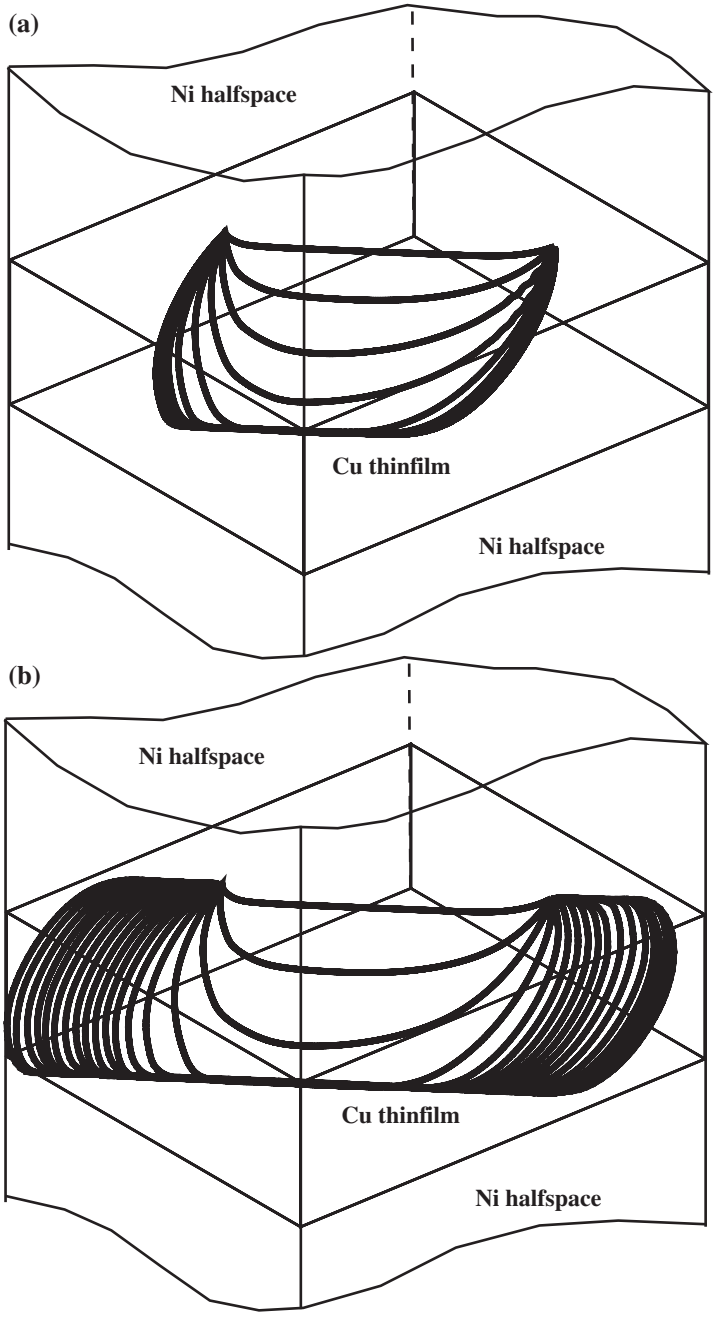

Figure 4. Dislocation motion in a thin layer with $h = 144\,\text{nm}$ under different applied biaxial stress levels (a) $\sigma_a = 210\,\text{MPa} < \sigma_c^{th} = 250\,\text{MPa}$, and (b) $\sigma_a = 280\,\text{MPa} > \sigma_c^{th} = 250\,\text{MPa}$. Each line corresponds to a time increment of 0.1 ns.

equation (47)), the dislocation will bow out in the Cu layer towards the interface. As a result of the image force exerted by the harder Ni layer, the dislocation is repelled away from the interface and reaches an equilibrium configuration. If the applied stress is larger than the critical value, the dislocation first bows out towards the interface then it is blocked by the image force and is confined to propagate within the layer. The critical stress for the onset of confined layer slip is first estimated according to equation (47) with equivalent isotropic values of μ and ν. This value is then refined by increasing (or decreasing) the applied stress until the dislocation can no longer achieve its equilibrium configuration.

The influence of the dislocation source size is also considered. Below the critical stress for threading dislocation motion, σ_c^{th}, dislocations cannot propagate in the layer. When the initial source size is larger than the layer thickness, the dislocation bows out and reaches an equilibrium configuration. If the initial source size is smaller than the layer thickness, slip propagation is controlled by the Orowan mechanism, and the critical stress for bowing out can be estimated as [41] $\sigma_c^{O} \approx (\mu b/2\pi L)(6)^{1/2} \ln(L/r_0)$.

In comparing the critical stresses for a threading dislocation motion within a layer, σ_c^{th}, with that for the activation of a F–R source by the Orowan mechanism, σ_c^{O}, the two values are close when the layer thickness, h, is on the order of the initial F–R source length, L. In any thin layer, many F–R sources may exist with different sizes, locations and orientations. If the applied stress is smaller than the critical stress for threading dislocation motion, $\sigma < \sigma_c^{th}$, some dislocations will expend towards the interface, but none would be able to propagate within the layer. Once the applied stress is removed, F–R source dislocations will re-tract to their original length. This type of dislocation motion does not lead to permanent deformation of the thin film. We term this regime as *quasi-elastic*. When the applied stress reaches the critical value σ_c^{th}, longer dislocations with $L > h$ will expand, but will still be confined within the layer. This regime of behaviour is the so-called confined layer slip (CLS) [35]. Finally, if the applied stress is increased further, $\sigma > \sigma_c^{O} > \sigma_c^{th}$, shorter dislocations $L < h$ are gradually activated, first bowing out from stable shapes, then reach the interface, and finally propagate within the layer. Thus, dislocations emitted from longer F–R sources with $L > h$ are controlled by the threading dislocation mechanism, while shorter ones by the Orowan mechanism.

4.2. *Loss of slip confinement*

As individual layers become very thin (i.e. in the tens of nanometers), only single dislocations can propagate and expand upon the application of an externally applied stress. However, because the layer thickness is very small, the curvature of the dislocation loop in segments subtended between layers would be extremely high, and thus self-forces in these regions are very substantial. The externally applied stress would have to overcome such large self-forces if these curved segments are to expand. The applied P–K force on those segments that are parallel to the interface does not have to overcome self-forces because the curvature of these segments is small. Rather, the image force from neighbouring and other interfaces would have to be overcome by the applied P–K force. Since we regularized the solution by selecting a cut-off radius of one Burgers vector on either side of the interface, the dislocation

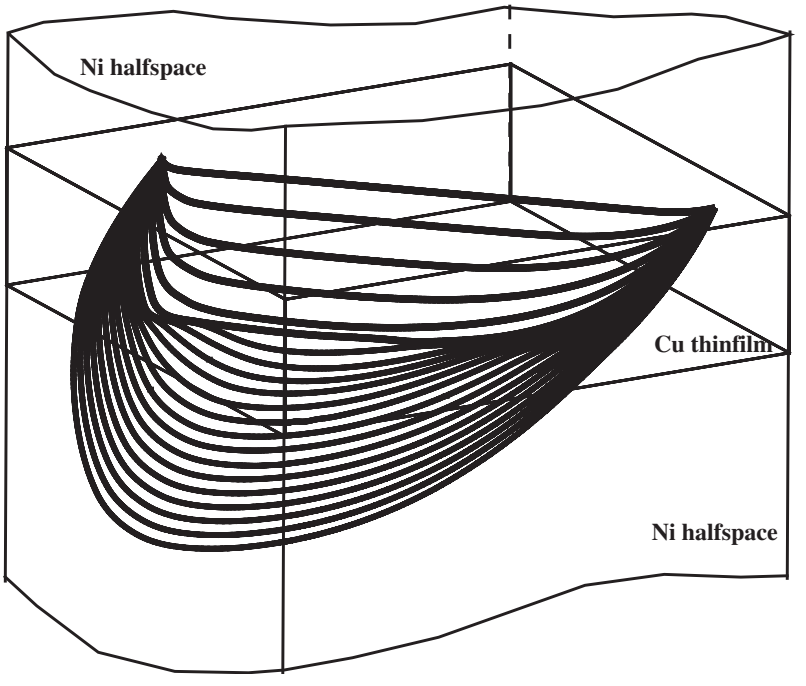

Figure 5. Dislocation motion in a thin layer with $h = 10.8\,\text{nm}$ under an applied stress $\sigma_a = 1.2\,\text{GPa} > \sigma_c^{th} = 1\,\text{GPa}$. Each line corresponds to a time increment of 2 ps.

will be repelled with a maximum image force on one side of the interface, and then attracted with a different maximum force once it crosses the interface. If the applied stress is high enough that the maximum P–K force on the straight dislocation segments close to the interface overcomes both repulsive and attractive forces, the dislocation will cross from one layer to the neighbouring one, and CLS is finally lost. This mode of deformation is shown in figure 5, where successive dislocation positions at 10 ns time intervals are shown for a F–R source dislocation, initially with a straight segment pinned at both ends, and is subjected to a suddenly applied bi-axial stress of magnitude 1.2 GPa. The dislocation, which lies on the (111)-slip plane, has an initial length of 43.2 nm, and its Burgers vector is $(a/2)[\bar{1}01]$. After 15 ps, the leading edge of the bowed out dislocation reaches the interface. Since the applied P–K force is larger than both the attractive and repulsive components of the image force, the dislocation loses confinement within the copper layer and expands into the neighbouring nickel layer.

Figure 6 shows results of our calculations for the maximum strength of a copper layer in a thin film of alternating Cu/Ni layers based on the activation of a single F–R source, as a function of the layer period. Experimental results for nano-indentation by Misra *et al.* [20] and Clemens *et al.* [34] are also shown. Since Freund's formula is often used to estimate the strength of thin films, film strength using equation (47) is also shown as a solid line in the same figure

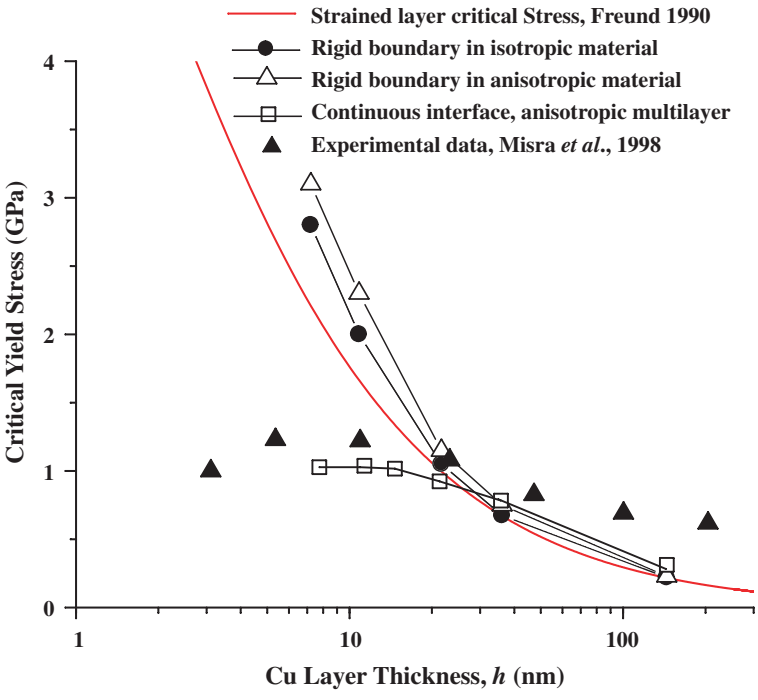

Figure 6. Yield strength of a Ni–Cu layered thin film as a function of the layer thickness. Solid line, Freund's formula [38]; solid triangles, experimental results of Misra *et al*. [20]; open triangles, rigid boundary of anisotropic material; solid circles, rigid boundary of isotropic material; and open squares, current multilayer anisotropic material with continuous interface.

for comparison. In this figure, open triangles are the results of calculations with rigid boundary conditions of an anisotropic material, while solid circles represent the results when rigid boundary conditions of the corresponding isotropic material are used, as is assumed in recent work on thin films [11]. Finally, open circles are the results of the current model for the multilayer anisotropic material with continuous interface conditions.

For layers of thickness less than approximately 100 nm, a single F–R source will determine the overall strength of the layer as a competition between confinement in the layer by image forces generated by elastic modulus mismatch, and resistance to deformation by self-forces on the curved ends of the dislocation loop. If the modulus mismatch is not too great, dislocation loops will cross from layer to layer rather than be confined within a layer. One would expect that the maximum strength is determined by the layer thickness and the ratio of elastic moduli as well. For thicker layers, F–R sources can operate many times leading to dislocation multiplication and the formation of a pile-up. In such a case, the dominant deformation mode is the Hall–Petch mechanism.

Based on the present simulations, a strength–thickness map for Cu/Ni multilayer materials is shown in figure 7. Four regions representing different

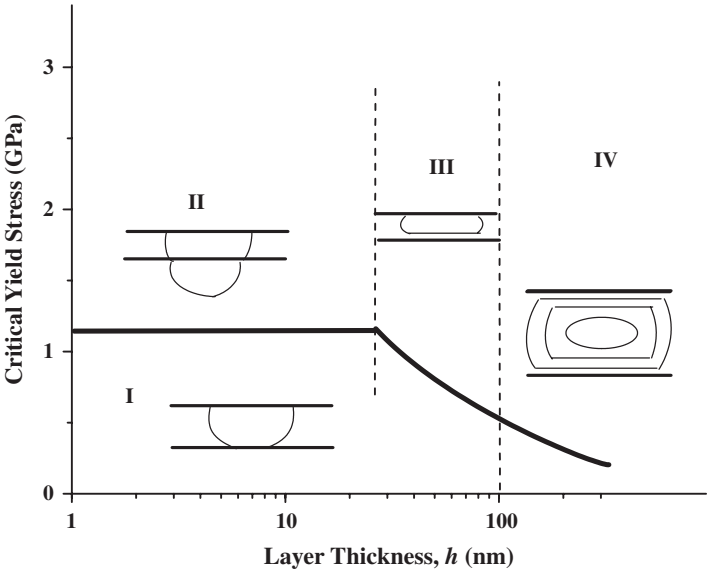

Figure 7. Plastic deformation mechanism and strength map for thin layered Cu/Ni films.

deformation mechanisms are shown, consistent with earlier investigations [21, 42]. These are:

1. *Region I*. The applied P–K force is smaller than both the Koehler barrier and the self-force. Dislocation loops deform to an equilibrium shape, and regain their original shape upon removal of the applied stress. This is a *quasi-elastic* deformation mode.
2. *Region II*. The applied P–K force is larger than the Koehler barrier. Dislocation loops are no longer confined in this region, and *plastic instability* is manifest in loss of confinement.
3. *Region III*. The applied P–K force is less than the Koehler barrier but still greater than the maximum self-force anywhere on the loop. Loops are forced to propagate within one layer in this *confined layer slip* (CLS) mode of deformation.
4. *Region IV*. The layer thickness is so large that it can support several emitted dislocations from F–R sources within the layer, but the applied P–K force is such that the leading dislocation in the pile-up cannot overcome the Koehler barrier. This is the *classical Hall–Petch* mode of plastic deformation.

5. Summary and conclusions

The development of a line integral form for the elastic field of dislocations in anisotropic, multilayered materials has enabled an extension of the PDD method to the simulations of plasticity and strength in these material systems. Earlier efforts in this area rely on surface integrals for the derivatives of Green's functions, which complicates numerical implementation in DD computer simulation programs.

The following conclusions can be drawn from applications of the developed method to a number of material deformation problems at the nano-scale to the micro-scale.

(i) The influence of free surfaces or interfaces on dislocation motion through image forces extends into the material to several hundred lattice constants. Thus, for computer simulations of large material volumes (e.g. tens of microns), image forces can be neglected until the dislocation is within a few hundred lattice constants. Numerical resolution of any method (including the Finite Element) must be sufficient close to the surface.

(ii) To retain the original idea of the dislocation self-force in an infinite medium, the elastic field is separated into two components: one that yields the self-force in an infinite medium, while the second is due to the effect of interfaces (i.e. the image force).

(iii) In thin Al films on Cu substrates, it is shown that a small layer of aluminium oxide can reverse the surface image force from attractive to repulsive. Also, the interaction between the Al/Al_2O_3 interface and the Al/Cu interface can result in near zero image force on curved dislocation segments in the middle of the film. If the oxide film thickness is greater than the film thickness itself, its image force can be approximated by the semi-infinite half-space results.

(iv) Plastic deformation of very thin layers in the tens of nanometers thickness range is controlled by a competition between the resistance of curved segments due to high self-forces, and the maximum force to transmit nearly straight segments across the interface (i.e. the Kohler barrier). If the layer is too thin, this results in high curvatures and resistance to CLS. Depending on the ratio of the elastic moduli of adjacent layers, dislocations may find an easier path to move into adjacent layers, and thus CLS is lost. On the other hand, if the ratio of elastic moduli between adjacent layers is sufficiently high and the layer thickness is sufficiently large, dislocations are forced to be confined within one layer.

(v) Strength calculations from the present model show reasonable agreement with experimental nano-indentation data on Cu/Ni nanolayered materials. Strength saturation below layer thicknesses of $\sim$20 nm is a result of the near independence of the Koehler barrier strength on layer thickness. The present model is incapable of explaining the decrease in layer strength below $\sim$10 nm, as shown in the experimental data. This limitation may be attributed to atomistic dislocation core effects not included in the model.

(vi) Four general deformation mechanisms are identified for layered thin films: quasi-elastic, plastic instability, confined layer slip, and the Hall–Petch regime, consistent with recent literature [21, 42].

Acknowledgements

We acknowledge the support of the U.S. National Science Foundation (NSF) for this research, through grant No. DMR-0113555, and the support of the U.S. Air Force Office for Scientific Research (AFOSR), through grant No. F49620-03-1-0031, with UCLA.

References

[1] L.P. Kubin, G. Canova and M. Condat, *et al*., Diffusion and Defect Data—Solid St. Data, Part B (Solid St. Phenomena) **23/24** 455 (1992).
[2] H.M. Zbib, M. Rhee and J.P. Hirth, Int. J. Mech. Sci. **40** 113 (1998).
[3] K. Schwarz, J. appl. Phys. **85** 108 (1999).
[4] N.M. Ghoniem, S.-H. Tong and L.Z. Sun, Phys. Rev. **61** 913 (2000).
[5] J. Lothe, V. Indenbom and V. Chamrov, Phys. Stat. sol. (b) **11** 671 (1982).
[6] D. Weygrand, L. Friedman, E. Van der Giessen, *et al*., Modeling Simul. Mater. Sci. Engng **10** 437 (2002).
[7] T. Gosling and J. Willis, J. Mech. Phys. Solids **42** 1199 (1994).
[8] M. Fivel, T. Gosling and I. Groma, Modeling Simul. Mater. Sci. Engng **4** 581 (1996).
[9] M. Verdier, M. Fivel and I. Groma, Modeling Simul. Mater. Sci. Engng **6** 755 (1998).
[10] T. Khraishi, H. Zbib and T. de la Rubia, Mater. Sci. Engng A **309/310** 283 (2001).
[11] B. von Blanckenhagen, P. Gumbsch and E. Arzt, Modelling Simul. Mater. Sci. Engng **9** 157 (2001).
[12] R. Martinez and N. Ghoniem, J. comp. Mater. Sci. **23** 225 (2002).
[13] X. Han, N. Ghoniem and Z. Wang, Phil. Mag. A **83** 3705 (2003).
[14] D. Bacon and P. Groves, *Fundamental Aspects of Dislocation Theory*, NBS Special Publication 317, Vol. 1, edited by J. Simmons, R. de Witt and R. Bullough (U.S. National Bureau of Standards, Washington, 1970), pp. 35–45.
[15] N. Salamon and J. Dundurs, J. Elasticity **1** 153 (1971).
[16] M. Comniou and J. Dundurs, J. Elasticity **5** 203 (1975).
[17] T. Mura, *Micromechanics of Defects in Solids*, 2nd edition (Martinus Nijhoff, Dordrecht, 1987).
[18] X. Han and N. Ghoniem, Phil. Mag. **85** 1205 (2005).
[19] T. Mitchell, Y. Lu, A. Griffin, *et al*., J. Am. Ceram. Soc. **80** 1673 (1997).
[20] A. Misra, V. Verdier, Y. Lu, *et al*., Scripta mater. **39** 555 (1998).
[21] P. Anderson, T. Foecke and P. Hazzledine, MRS Bull. **20** 27 (1999).
[22] J. Embury and K. Han, paper presented at the Eighth International Conference on the Mechanical Behavior of Materials, Victoria, Canada (1999).
[23] H. Kung and T. Foecke, MRS Bull. **24** 14 (1999).
[24] J. Embury and J. Hirth, Acta metall. mater. **42** 2051 (1994).
[25] B. Yang and E. Pan, Int. J. Solids Struct. **39** 2235 (2002).
[26] T. Ting, *Anisotropic Elasticity: Theory and Applications* (Oxford University Press, New York, 1996).
[27] J. Hirth and J. Lothe, *Theory of Dislocations*, 2nd edition (Wiley, New York, 1982).
[28] E. Pan and F. Yuan, Int. J. Solids Struct. **37** 5329 (1999).
[29] B. Yang and E. Pan, Engng Anal. Boundary Element **26** 355 (2002).
[30] R. Hill, in *Progress in Solid Mechanics 2*, edited by I. Sneddon and R. Hill (North-Holland, Amsterdam, 1961), pp. 245–276.
[31] L. Brown, Phil. Mag. **10** 441 (1964).
[32] S. Gavazza and D. Barnett, J. Mech. Phys. Solids **24** 171 (1976).
[33] C. Sinclair, J. Embury and G. Weatherly, Mater. Sci. Engng A **272** 90 (1999).
[34] B. Clemens, H. Kung and S. Barnett, MRS Bull. **20** 20 (1999).
[35] P. Anderson and Z. Li, Mater. Sci. Engng A **319–321** 182 (2001).
[36] S. Rao and P. Hazzledine, Phil. Mag. A **80** 2011 (2000).
[37] B. Daniels, W. Nix and B. Clemens, in *Thin Films: Stress and Mechanical Properties V*, Materials Research Society Symposium Proceeding 356, edited by S. Baker, C. Ross, P. Townsend, *et al.* (Materials Research Society, Pittsburgh, 1995), pp. 373–378.
[38] L. Freund, J. Mech. Phys. Solids **58** 657 (1990).
[39] W. Nix, Scripta mater. **39** 545 (1998).
[40] D. Rodney and R. Phillips, Phys. Rev. Lett. **82** 1704 (1999).
[41] A. Foreman, Phil. Mag. **15** 1011 (1967).
[42] A. Misra, V. Verdier, H. Kung, *et al*., Scripta mater. **41** 973 (1999).